Friction and Adhesion between C_{60} Single Crystal Surfaces and AFM Tips: Effects of the Orientational Phase Transition

Q. Liang,[†,‡] Hongnian Li,[§] Yabo Xu,[§] and Xudong Xiao*[,†]

Department of Physics and Institute of Nano Science and Technology, The Hong Kong University of Science and Technology, Hong Kong, China, Instrumental Analysis Center, Shanghai Jiaotong University, Shanghai, China, and Department of Physics, Zhejiang University, Hangzhou, Zhejiang, China

Received: September 1, 2005; In Final Form: October 21, 2005

We have investigated the nanotribological properties of C_{60} single crystal (111) and (100) surfaces around its orientational order−disorder phase transition temperature, ∼260 K, by atomic force microscopy and frictional force microscopy (AFM/FFM) in high vacuum. Results show that for both surfaces across the phase transition temperature, the friction force and the adhesive force between a C_{60} coated AFM tip and the C_{60} crystal surfaces exhibit discontinuous behavior. The friction force within the applied external load range in the low temperature phase is significantly larger than that in the high temperature phase, with no obvious change in the slope of the friction force curves (the friction coefficient) in the low and high temperature phases. The abrupt change in friction was found to be caused mainly by the abrupt change in adhesion, which, in turn, can be qualitatively understood through changes in the van der Waals interaction and the short-range Coulomb interaction associated with the structural changes across the phase transition. Compared to most other degrees of freedom, the rotation of C_{60} molecules was found to have little effect on friction and is an ineffective energy dissipation channel.

1. Introduction

It is well known that carbon atoms can form three common structures: graphite, diamond, and fullerene.[1] Unlike the first two, which are infinite periodic network solids, the third form of carbon is a molecular form, which are hollow and geodesic spheroids.[2] The C_{60} molecule, also called the buckminsterfullerene, consists of 20 hexagons and 12 pentagons in the dome and has the highest possible symmetry of any molecule that has taken the shape of soccer ball. The two characteristic interatomic distances within a C_{60} molecule are 0.140 nm between two carbon atoms shared by adjacent hexagons and 0.145 nm between two carbon atoms shared by a hexagon and a pentagon. This 0.71 nm diameter[3] C_{60} molecule displays many unusual physical, chemical, and electronic properties due to its special molecular structure.

At room temperature (RT), C_{60} molecules can form well-ordered face-centered-cubic (fcc) molecular crystals. For each simple cubic (sc) unit cell, there are four molecules and each molecule rotates at a high frequency while remaining in its own lattice position. Since each C_{60} molecule is constantly changing its orientation every 10^{-11}s,[4] all the molecules in the unit cell are equivalent for measurement that requires a time longer than the rotational period. Thus, the pertinent space group for the crystal structure is $Fm3m$.

When the crystal is cooled to around 260 K, an orientaional ordering phase transition from the fcc to the sc lattice structure occurs.[5] The C_{60} balls retain their former lattice positions in the newly contracted fcc arrangement, but they are no longer identical because the four C_{60} molecules associated with the primitive cubic cell each have their own specific orientations around four equivalent but different ⟨111⟩ directions. The situation is further complicated by the fact that these large near-spherical C_{60} molecules can still rotationally hop between two distinct orientations with similar energy around the ⟨111⟩ axis.[6,7] Only at about 90 K, does this C_{60} molecular rotational hopping come to a full stop with the molecules' orientations around the ⟨111⟩ directions frozen.[8] When the orientational ordering phase transition occurs, many physical and chemical properties can change, accompanied by the change of the crystal structure (symmetry).

Although frictional forces play a vital role in daily life and are easily measured, the fundamental mechanisms of friction on the micro- and molecular scales are still poorly understood.[9−11] It is well known that thin layers of certain materials can drastically reduce the friction of surfaces.[12] Soon after the discovery of the C_{60} molecule, there was speculation about the possible unique lubricating properties of C_{60} films due to the nearly spherical shape of individual C_{60} molecules. According to classical mechanics, spherical balls between two moving bodies can act as lubricants through the exploitation of low rolling friction.[13] Analogously, C_{60} molecules were expected to work like nanoscale ball bearings and the rolling motion of these 0.71 nm large, rigid spheres was anticipated to greatly reduce friction against any mating objects in relative motion. But this expectation was not borne out by either microscopic or macroscopic experiments.[14−21] The best friction result between two C_{60} films has a friction coefficient of ∼0.15, which is much greater than the friction coefficient of graphite (0.01).[22] In any case, C_{60} solid provides a good system to study the

* Corresponding author. Department of Physics, Hong Kong University of Science and Technology, Clear Water Bay, Kowloon, Hong Kong, China. Tel: (852) 2358-7494; Fax: (852) 2358-1652; E-mail: phxudong@ust.hk.
[†] The Hong Kong University of Science and Technology.
[‡] Shanghai Jiaotong University.
[§] Zhejiang University.

10.1021/jp054939o CCC: $33.50
Published on Web 12/14/2005

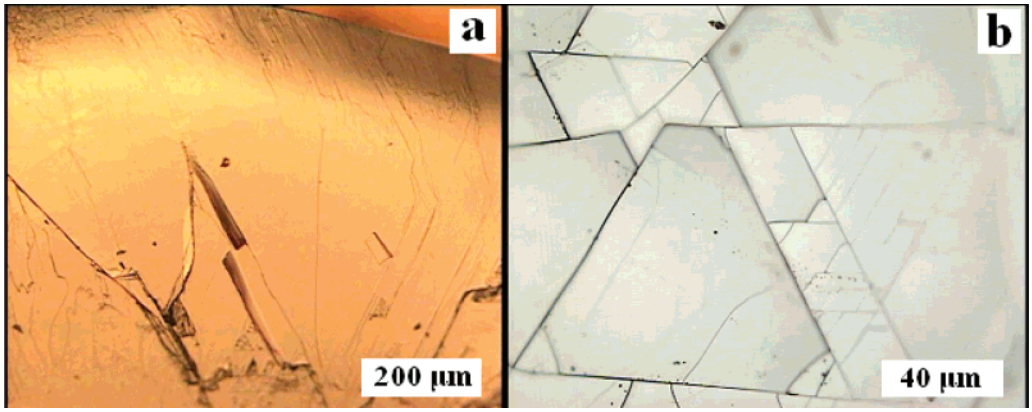

Figure 1. Optical microscopic images of the crystalline C_{60} sample surface at (a) a magnification of 100 times and (b) a magnification of 500 times. The regular triangles formed by the cracks due to thermal heating demonstrate that the surface is the (111) orientation.

mechanism of energy dissipation during frictional processes, which is the central question of tribological studies.[9,10]

Most previous studies[14−21,23] of the frictional properties of C_{60} were conducted on C_{60} thin film samples. The methods to obtain these films included vacuum sublimation from C_{60} powder,[16,17] Langmuir−Blodgett (LB)-like condensation,[24] magnetron sputtering,[19] and molecular beam epitaxy (MBE).[20] However, different films or film/substrate systems led to quite different and even contradictory frictional results. In the different samples used in the earlier experiments, there were certainly influences from the quality of the films and the lattice mismatch between the C_{60} films and the substrate. To avoid such uncertainties, we used C_{60} single crystals as our sample because these crystals have almost an ideal lattice. In particular, we performed our measurements by varying the sample temperature to explore the effect of the orientational ordering phase transition on the tribological properties. Part of our tribological results on the C_{60}(111) surface was already reported in an earlier letter;[25] here we include them with more detailed experimental information in order to compare with results on the C_{60}(100) surface. For both surfaces, results on the scanning velocity dependent friction will also be presented and discussed.

2. Experimental Methods

The experiments were carried out with a Seiko SPA 3800 atomic force microscope/frictional force microscope (AFM/FFM) with a cooling stage on the scanner (sample holder). The sample could be cooled to 150 K by liquid nitrogen. The chamber that hosted the AFM/FFM had a background pressure better than 7×10^{-7} Torr. Commercially available V-shaped Si_3N_4 cantilevers/tips with a nominal normal force constant of 0.1 N/m (Veeco Instruments, NY) were used to acquire images in the contact mode and to measure the adhesive and frictional forces. For most AFM cantilevers/tips used, both the normal force constant and the lateral force constant of the cantilevers were calibrated by well-established methods.[26] In some cases, when it was sufficient to have a relative comparison and the absolute friction value was not of our concern, we then left the lateral force constant of the cantilever uncalibrated and the frictional force in an arbitrary unit. As usual, a quadrant photodiode was used to measure both the normal force (cantilever deflection) and the frictional force (cantilever torsion) simultaneously. The value of the surface adhesion was obtained by measuring the force−distance curves through the pull-off force, and the friction was measured from the friction loop signals at each given external load.[22] By varying the external load sequentially, a friction force versus load curve, which is called the friction force curve in the latter part of this paper, was constructed. The normal load applied on the sample was changed through the applied voltage on the piezo tube, whose *X*, *Y*, and *Z* scales at different temperatures had been carefully calibrated in order to facilitate comparisons among the results obtained at different temperatures. The detailed description of friction and adhesion measurements can be found elsewhere.[27] To avoid the accumulative effect of surface wear, we changed the measurement spot on the sample continually.

Large C_{60} single crystals were grown from sublimed vapors by nucleation control through a proper time-dependent temperature procedure.[28] The raw materials, C_{60} powder of 99.9% purity or small single crystals, were first degassed at 530 K for 24 h in an evacuated quartz tube at high vacuum ($\sim 2 \times 10^{-7}$ Torr) and then purified by sublimation from the end to the middle section of the tube. The purified C_{60} materials in the middle section of the quartz tube ($\sim$20 cm) were then sealed off and placed into a horizontal tube furnace for crystal growth. Usually, there are a few nuclei in the growth zone. However, by a proper design of the temperature gradient along the furnace and a time-dependent control of the temperature at the cool end, we managed to eliminate or suppress the growth of most nuclei and to leave only the nucleus nearest to the cool end to grow larger. In this manner, high quality C_{60} crystals $\sim$1 cm in size were grown with exposed {111} and {100} surfaces.

The C_{60} single crystal was then cleaved in the ambient air, and immediately after cleavage it was put into the high vacuum chamber. Before the measurements, we heated the sample to 390 K for more than an hour to remove adsorbed impurities, e.g., water molecules, from the surface. The surface remained clean for tribological studies for about 20 h, after which reheating at 390 K for half an hour could recover the clean surface. At each temperature, because of the poor heat conductivity of C_{60} solid,[29] we waited for at least half an hour to reach the thermal equilibrium between the sample and the cooling stage.

3. Results and Discussion

3.1. Molecularly Resolved Images of C_{60}(111) Surface. Figure 1 shows two optical microscopic images of a newly cleaved surface of a C_{60} (111) sample with a magnification of about 100 and 500 times, respectively. This cleaved surface is atomically flat and can be imaged by AFM. Figure 1b shows that after light illumination, especially after exposure to laser beams, some cracks have developed on the surface due to thermal heating.[30,31] The sample displays many regular triangles that demonstrate the ⟨111⟩ orientation of the C_{60} crystal lattices.

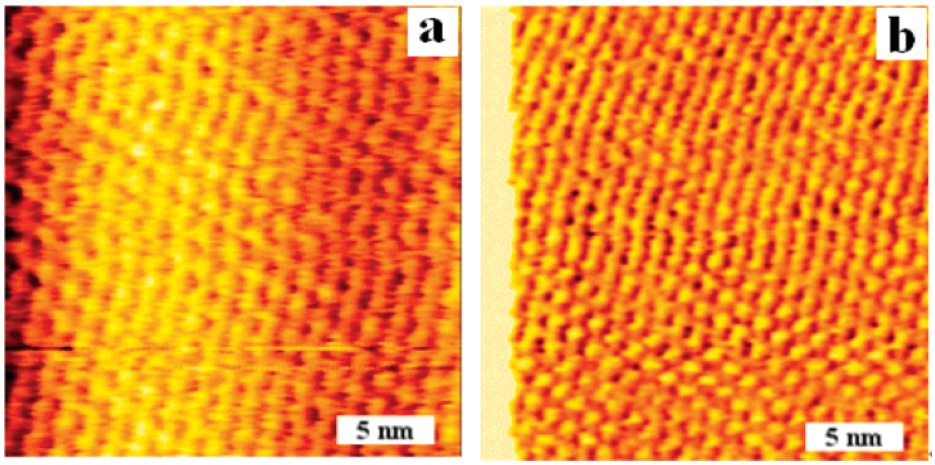

Figure 2. Molecular-resolved images of the C_{60}(111) surface at 2 nN external load: (a) topographic image and (b) frictional image.

We have also obtained molecular-resolved topography of the C_{60} crystal surface using contact-mode AFM (Figure 2), indicating the high quality of sample. The images in Figure 2a and b correspond to topographic and frictional images, respectively. Generally, it is easier to obtain a molecularly resolved frictional image than the topographic image, perhaps due to the stiffer lateral force constant with less noise. In the images, the expected hexagonal structure formed by the C_{60} molecules is clearly observable, showing a nearest neighbor distance of about 1 nm. Although the C_{60} molecules are nearly freely rotating at a very high speed, their spatial positions remain at the fcc sites. Below the phase transition temperature of ~260 K, even though an abrupt shrinkage of the lattice constant by ~0.34% exists, the limited sensitivity of the AFM does not allow us to detect such a small distance change in the lattice.

3.2. Temperature-Dependent Friction. It is well known that the AFM tip is critically important in tribological measurements with AFM. This includes the tip radius, the tip shape, and the chemical composition on the tip surface.[32] To ensure the tip geometry, we treat the tip by carefully scanning on a cleaved mica surface at a relatively high load until a stable friction curve is obtained.[33] This procedure guarantees that the radius of curvature and shape of the tip will remain stable during the latter experiments at lower loads. In the present experiment, the tip radius was around 50 nm as checked by a commercial Nioprobe[34] sample and analyzed by the SPIP software.[35] On the other hand, we found that the C_{60} surface structure started to wear when the external load was about 15 nN, similar to the result for sublimated fullerene thin films.[14] Thus, to obtain a wearless friction measurement, we limited the maximum applied normal force to 10 nN to avoid damage of the C_{60} surface by the AFM tip. With these precautions, the measured friction force versus the external load curves at a sliding speed of 1.5 μm/s for both (111) and (100) surfaces are shown in Figure 3a and b, respectively. Obviously, the results at various temperatures between 250 K and room-temperature fall into two groups: those below (solid symbols) the phase transition temperature of ~265 K have a higher friction force than those above (open symbols) the phase transition temperature. The abrupt change in the friction force appears in both crystal surfaces. The phase transition temperature corresponding to this abrupt change is around 260~265 K, consistent with previous results.[5] Friction force curves above and below the phase transition temperature have very similar slopes but with a large different offset at zero external load. At a given load, the ratio of the two friction force values for the two phases is about 1.5. To discern that this observed temperature effect is not induced by our instrument,

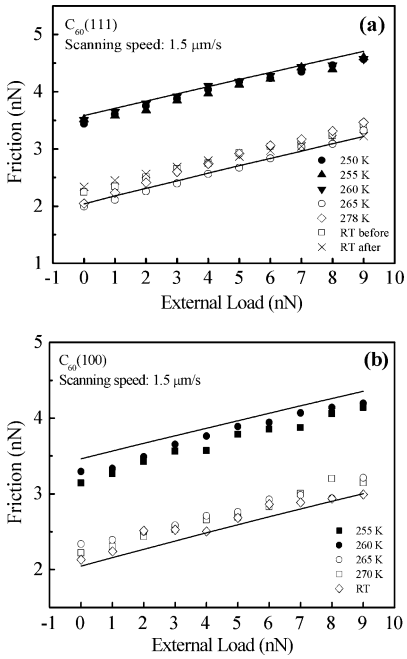

Figure 3. Friction versus external load curves for a (a) C_{60}(111) surface and a (b) C_{60}(100) surface at a number of temperatures above and below the orientational order-disorder phase transition temperature. The solid lines indicate fitting by the JKR model (eq 3) with the measured adhesion force at the two phases.

we used the same procedure for changing temperature on two reference samples (using a clean Si_3N_4 tip): newly cleaved mica and an oxidized Si (100) wafer. Both showed no significant temperature dependent friction. The results for mica are shown in Figure 4. Considering the experimental errors, the friction force curves remain basically unchanged from 240 K to room temperature, demonstrating that the fcc-to-sc phase transition of crystalline C_{60} is responsible for the observed abrupt change of friction on C_{60} surfaces.

In general, an AFM tip can be chemically modified by the sample material and this chemical modification will influence the frictional and adhesive behaviors between the tip and the sample surface.[33] Unfortunately, the amount of transferred material on the tip apex is very small due to its small area (~10 nm^2). It is therefore difficult to identify the structure and property of the chemical modification. With a clean Si_3N_4 tip, we found that the C_{60} molecules easily adhere to the tip surface and cause the tip to be covered by C_{60}, as depicted in Figure 5. The evidence for the C_{60} transfer comes from the frictional force

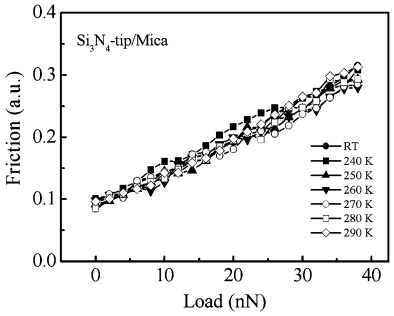

Figure 4. Friction versus load curves at different temperatures for a Si_3N_4-tip scanning on mica using the same instrument. Results are nearly temperature independent.

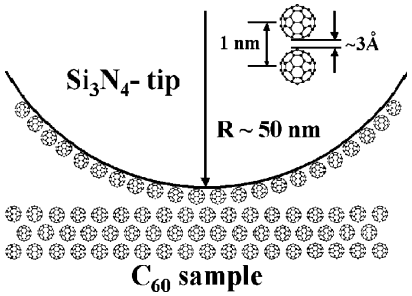

Figure 5. Schematic showing the contact between a C_{60} covered tip and a C_{60} crystal surface.

data. When starting with a clean Si_3N_4 tip scanning on a C_{60} solid surface, the frictional data at the beginning are divergent and the friction force curves are unstable. After a number of friction scans, the friction force curves eventually become stable and reproducible. At this stage, the AFM tip has clearly become covered with a layer of the sample materials as indicated by the friction force curve on the clean mica surface, which is obviously different from the curves against a clean AFM tip. This modification process is similar to tips treated with poly(tetrafluoroethylene) (PTFE)[36] or with alkanethiol molecules[37] to obtain rather stable tips. The stable friction force curves with the C_{60}-modified AFM tip indicate that the two relative moving surfaces remain unchanged, i.e., the reported frictional study (Figure 3) is between a C_{60}-modified tip and a C_{60} solid surface. Further check of the stability of the C_{60}-modified tip is carried out by repeating the friction measurements at room temperature before and after the experiment. While definitive structural information on the C_{60} layer on the AFM tip is not available, we suspect it includes a flake of the sample material.

3.3. Temperature-Dependent Adhesion and Its Influence on Friction. In general, surface adhesion could significantly influence frictional properties at the molecular scale. To understand the adhesive property is thus very important in friction studies. For this reason, we measured the adhesion force between the C_{60}-modified tip and the C_{60} surface via normal force−distance curves. The temperature-dependent adhesion forces for (111) and (100) surfaces are plotted in Figure 6a and 6b, respectively. As the figure shows, while the adhesion force below the phase transition temperature is ~18 nN, it decreases abruptly to ~9 nN above the phase transition temperature. The values for both sample surfaces are similar. To check the reversibility of this jump, we switched the temperature of the (111) sample between 260 K and 270 K a number of times and measured the resulting adhesion at several different positions for each temperature. The results, shown in the inset to Figure 6a, verify the reversibility of the jump. The deteriorated reproducibility over a 10-h time scale is due to adsorption of water and other impurities in the chamber. The adhesion value

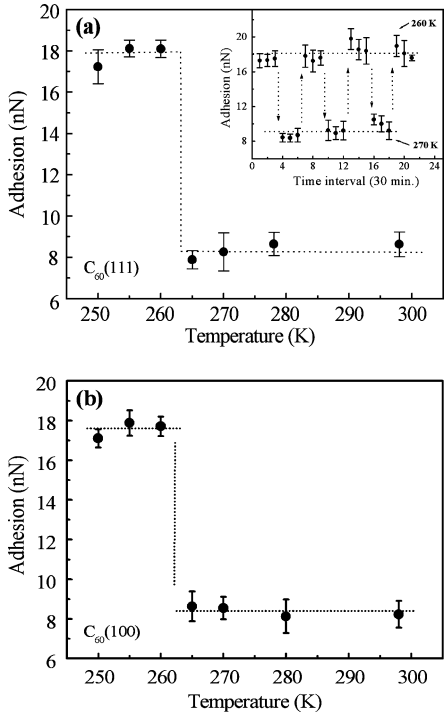

Figure 6. Abrupt change of adhesion force around the phase transition temperature (a) for C_{60}(111) and (b) for C_{60}(100). The inset in (a) demonstrates the reversibility of the measurement in about 10 h.

at room temperature is consistent with several previously reported measurements for C_{60} films on GeS[15] and C_{60} monolayers on self-assembled monolayers (SAM).[38] To rule out instrumentation artifacts, a control experiment of the adhesion force between a clean Si_3N_4 tip and the oxidized Si (100) wafer surface, and between a clean Si_3N_4 tip and newly cleaved mica, was performed. The constant adhesion from 250 K to room temperature indicates that the observed effect on C_{60} is a specific property induced by the phase transition.

Because the experiment is performed in high vacuum, the effect of the capillary force between the tip and the surface can be ignored. The adhesion force between the tip and the sample surface must mainly come from the van der Waals interaction. Here, we applied the JKR model[39] to simulate our data and to show that an abrupt change in adhesion can induce an abrupt change in friction.

Assuming that the contact area between the AFM tip and the C_{60} sample surface is A and the shear strength, τ, takes the form $\tau = \tau_0 + \alpha P$, the friction force, F_f, is given by[40]

$$F_f = (\tau_0 + \alpha P)A \tag{1}$$

where τ_0 and α are constants and P is the pressure. We calculate A using the JKR model, in which the contact radius, a, is given by[15,41]

$$a^3 = \frac{R}{K}[L + 2L_a + 2\sqrt{L_aL + L_a^2}] \tag{2}$$

where L and L_a are the external load and adhesion force respectively, R is the tip radius and K the effective elastic modulus. One can derive the friction force as[15]

$$F_f = \alpha(L + L_a) + \tau_1(\sqrt{L + L_a} + \sqrt{L_a})^{4/3} \tag{3}$$

where τ_1 is a constant that is proportional to τ_0, $\tau_1 = \tau_0\pi(R/K)^{2/3}$. When using the adhesion force, L_a, as measured and setting

either $\alpha = 0$ or $\tau_1 = 0$, eq 3 cannot fit the data in Figure 3a and b. This indicates that the shear strength of the contact must be pressure dependent ($\alpha \neq 0$) and the simple Amonton's law,[40] even with a modification in the total load, does not apply ($\tau_1 \neq 0$). The two solid curves in Figure 3a are fittings with $\alpha = 0.092$ and $\tau_1 = 0.11$ nN$^{1/3}$; in Figure 3b they are fittings with $\alpha = 0.058$ and $\tau_1 = 0.14$ nN$^{1/3}$. Taking $R \sim 50$ nm and $K \sim 15$ GPa (estimated from the elastic modulus of solid C_{60}), we arrive at $\tau_0 \sim 0.017$GPa for Figure 3a and 0.020 GPa for Figure 3b, much smaller than the values deduced for C_{60} monolayer on GeS.[15]

The fact that the same set of parameters can reasonably fit the friction data both below and above the phase transition temperatures implies that our observed abrupt friction change is mainly induced by the adhesion force change, that is, it is due to the change in contact area. Only minor effects, which presumably account for the deviations between the data and the solid fitting lines, originate from the shear strength (friction coefficient) change across the phase transition. A close inspection of Figure 3 indicates that the solid fitting curves consistently over-estimate the friction difference by about 15% across the phase transition as compared with the experimental data. Using the high-temperature results as a reference, the measured friction below the phase transition temperature is smaller than what it would be if adhesion were the sole effect from the phase transition. Since electronic and phononic contributions across this phase transition are not expected to change very much, we conclude that hindrance of the C_{60} molecular rotation may lower the friction to a small extent. In other words, the rotational degree of freedom of C_{60} molecules, although not significantly contributing to the observed abrupt friction change across the phase transition, may still participate in the energy dissipation in the friction process to a small degree.

Microscopic mechanisms for energy dissipation in wearless friction have been the topic of many studies since the invention of friction force microscopy (FFM) and the quartz crystal microbalance technique (QCM). For solid surfaces, the contributions to friction from the excitation of electrons and phonons have been investigated. Using QCM, it was found that the friction force between a Pb film and a solid N_2 drops abruptly by a factor of 2 as Pb becomes superconducting.[42] This was taken as strong evidence for electronic excitation being an important energy dissipation channel, although doubts were raised later by the failure to reproduce this result by another group.[43] A dominant phonon contribution of at least 75% of the total friction was also demonstrated for solid Xe layers on Ag(111).[44,45] In molecular systems, excitation of other modes such as molecular bending and gauche kink excitation was also shown to dissipate energy effectively. The pressure induced tilt of alkylsilane molecules in a self-assembled monolayer was found to increase friction force by a factor of as much as 5.[46] In a recent study, we found that creation of gauche kinks in self-assembled alkanethiol monolayers on Au(111) can increase the friction force by as much as 10 times, depending on the monolayer density.[11] Compared with these highly effective energy dissipation channels, our above results on C_{60} surfaces indicate that molecular rotation is a very inefficient energy dissipation channel.

3.4. Microscopic Mechanisms of Adhesion Change. As presented above, the contact in our experiment is between C_{60} and C_{60}, instead of Si_3N_4 and C_{60}. The phase transition that changes the behavior of C_{60} molecular rotation does not significantly affect the shear strength (the friction coefficient). The abrupt change in the friction can be mainly attributed to the change in adhesion. Understanding the adhesion change becomes the key issue in understanding our results.

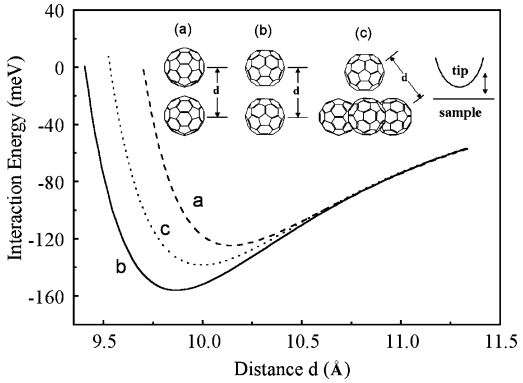

Figure 7. Calculated van der Waals interaction energies between two C_{60} molecules for a number of geometries. The interaction energy minima are assumed to correspond to the tip−sample contact. The inset shows models for (a) vertex-to-vertex, (b) hexagon-to-hexagon, and (c) double bond-to-pentagon center geometries.

Since our experiment was performed in high vacuum, the capillary force contribution to adhesion was negligible and the main contribution to adhesion between the C_{60}-modified AFM tip and the crystalline C_{60} surfaces was from the van der Waals force and the short-range Coulomb interactions,[47] due to the nonuniform distribution of charges over the C_{60} sphere. Because of the hollow structure and the large diameter of C_{60} molecules, the continuum theory that uses macroscopic properties to compute the van der Waals force must fail.[18,41] We must use microscopic theory to understand the adhesion between the two contacting surfaces.

The $C_{60}-C_{60}$ interaction between two molecules consists of the van der Waals interaction and short-range Coulomb interaction:[47,48]

$$V = \sum_{i,j=1}^{60} 4\epsilon\left[\left(\frac{\sigma}{r_{ij}}\right)^{12} - \left(\frac{\sigma}{r_{ij}}\right)^{6}\right] + \sum_{m,n=1}^{90} \frac{q_m q_n}{R_{mn}} \qquad (4)$$

where $\epsilon = 2.964$ meV, $\sigma = 3.407$ Å, r_{ij} is the distance between the ith C atom in the first molecule and the jth C atom in the second molecule, R_{mn} is the distance between the bond center of the mth bond in the first molecule and the bond center of the nth bond in the second molecule, and $q_{m,n}$ are the effective bond charges. Two factors may account for the decrease in adhesion in the fcc phase as compared with that in the sc phase: (i) in the fcc phase, all C_{60} molecules are rotating at fast speed, which would wash out the short-range Coulomb interaction; (ii) because of the fast rotation in the fcc phase, the distance between the two neighboring C_{60} molecules is somewhat larger, which results in smaller van der Waals interactions. The random orientation of the two molecules further decreases the overall van der Waals interaction as compared with a given orientation geometry. The second effect is demonstrated clearly in Figure 7, where the van der Waals interaction energies for a few different orientational configurations are plotted. Quantitatively, we found an increased interaction energy by about 25% and a shorter $C_{60}-C_{60}$ distance by about 0.3 Å with a hexagon-to-hexagon geometry as compared to molecules with a vertex-to-vertex geometry. If the C_{60} molecules on the surfaces took the orientation as in the bulk, i.e., with the double bonds facing the centers of the pentagon in the sc phase, we found an interaction energy increase of only about 11% and a tip−sample distance shortening of about 0.15 Å. While it is difficult to estimate quantitatively the short-range Coulomb interaction energy due

to uncertainty in the modeling, the literature indicates the orientation-dependent interaction energy from various model calculations to be about 0.2−0.4 eV/molecule for crystalline C_{60}, which is quite significant when compared to the orientation-independent interaction energy (∼1.5−1.7 eV).[47,48] In the sc phase, with the double bonds in one C_{60} molecule preferentially facing the centers of the pentagons of the neighboring C_{60} molecules,[48] an increase of the attractive interaction energy and thus the adhesion would result if the C_{60} molecules on both the tip and sample adopted this optimally oriented configuration upon contact. In the fcc phase, the free rotation of C_{60} breaks such "bonds" and smoothes out the orientation-dependent part of the interaction, resulting in a reduction of adhesion.

A microscopic calculation to account quantitatively for our observed adhesion force change across the phase transition is beyond the scope of the present paper. First, the nature and structure of the C_{60} film on the tip side are unknown. We may speculate that it as a flake of a C_{60} layer transferred from the C_{60} crystal surface; however, it may take other forms such as partial C_{60} monolayer as well. Second, at the interface, the vertical separation between the C_{60} molecules does not need to maintain that of the crystalline bulk. These surface C_{60} molecules may find the best optimized positions as well as orientations to maximize the adhesive interaction during contact. For example, a hexagon-to-hexagon geometry would maximize the van der Waals interaction by allowing the AFM tip to get closer to the sample surface but unfortunately may not favor the short-range Coulomb interaction. The observed similar adhesion behavior for the two crystal surfaces, (111) and (100), seems to support that the orientations of the C_{60} molecules at the surface may not be identical as those in the bulk. Last, a full calculation must include all the molecules at the contact, which requires detailed information on the structure of the two contacting surfaces and on the relative positions of the molecules. Our argument and calculations are qualitatively in agreement with our experimental results, but a quantitative understanding of the adhesion change requires deeper understanding as well as further work.

3.5. Scanning Velocity Effect of Friction. The friction data presented above were obtained at a scanning velocity of 1.5 μm/s. One wonders whether the observed abrupt change in friction across the phase transition temperature depends on scanning velocity. A full measurement at 0.5 μm/s shows that all the qualitative features of the phenomenon remain unchanged although quantitative differences do exist. With other scanning velocities, v, from 100 nm/s to 2.4 μm/s, we explore such a behavior at a given external load (7 nN) and at two chosen temperatures, one at 255 K (sc phase), below the phase transition temperature, and the other at RT (fcc phase), above the transition temperature. According to our results in Figure 3, the orientational order−disorder phase transition of C_{60} solid induces an abrupt friction force change around 260−265 K, but within each phase the temperature dependence is negligible. The scanning velocity-dependent results are shown in Figure 8a for C_{60} (111) and in Figure 8b for C_{60} (100). We can see that the frictional force at each temperature shows a linear increase with the logarithm of the sliding velocity when the velocity is below 1 μm/s, but it reaches a saturation value when the velocity is higher than 1 μm/s. The abrupt change in the friction occurs over the entire velocity range. Despite these common features, the slopes of the curves at RT and 255 K are clearly different for each surface, and the behaviors of the slopes for the two surfaces are even opposite.

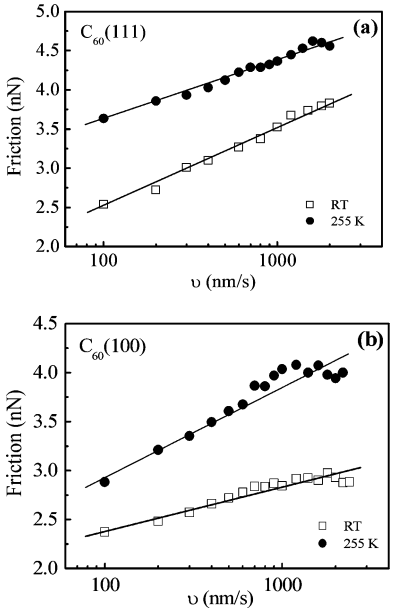

Figure 8. Friction of C_{60} surfaces versus scanning velocity (a) for C_{60}(111) and (b) for C_{60}(100). The solid lines are the linear fit of the friction to the logarithmic velocity.

On the molecular scale, the friction force has been reported to depend on the AFM scanning velocity in a number of systems.[49−52] Logarithmic velocity-dependent friction force was observed in quite a few systems, ranging from an atomically flat crystal surface to rough thin films. While the detailed mechanisms may differ, it was recognized that such velocity dependence is related to one kind or another of sliding discontinuity, with the average velocity matching the materials' intrinsic relaxation times.[52] From a thermodynamic point of view, the sliding discontinuities are caused by activation barriers, which are repeatedly overcome during the sliding process. For example, the logarithmic velocity dependence of friction on the atomically flat NaCl surface studied by Gnecco et al.[48] was interpreted to be due to the atomic stick-slip discontinuous motion originating from the tip-atom interaction potential with periodic barriers. On the micrometer scale, the velocity dependence of friction was studied in both triethoxysilane molecules and polymers grafted on silica, both of which showed a linear increase in the friction force with the logarithm of velocity up to $v = 300$ μm/s.[53,54] Even though the surface has no periodicity, the observed effect was interpreted as due to stick-slip motion originating from the molecular interaction with a stress modification. Once the sliding velocity exceeds a critical value, v_c, which has to do with the material's relaxation time and the AFM tip response, the thermal activation is no longer relevant and the friction force becomes velocity independent.[10] The critical velocity depends on several parameters, i.e., the amplitude of the tip−sample potential, the applied load, the temperature, and the characteristic frequency of the sample material. The transition from a static friction regime with logarithmic velocity dependence to a sliding friction regime with no velocity dependence was experimentally demonstrated on LB films within the velocity range 0.01 to ∼50 μm/s, with a critical velocity, v_c, of 3.5 μm/s.[55] Our observation of C_{60} crystals is consistent with the above pictures. Within the velocity range measured, we observed a transition from a logarithmic dependence to saturation, with a critical velocity of about 1 μm/s. However, the details of the friction behaviors in the two phases and on the two surfaces remain to be investigated in the future. The molecular rotation is clearly too fast to contribute to the

velocity dependence. However, the glassy state of C_{60} crystals in this temperature range as compared to a truly solid state at below 90 K may account for the characteristic relaxation.

4. Conclusions

In summary, we have studied nano-tribological and adhesive properties of two C_{60} single crystalline surfaces (111) and (100) across the phase transition temperature, ~260 K, by AFM/FFM in high vacuum. While friction and adhesion above or below the phase transition temperature, ~260 K, have very little temperature dependence, an abrupt jump across the phase transition temperature in both friction and adhesion for both surfaces was observed. The abrupt friction change was found to mainly originate from the abrupt adhesion change across the phase transition. Results show that at the low load (<10 nN), the friction is nearly linearly proportional to the applied load on the surface, but the slope of the friction curve, which represents the frictional coefficient, remains without obvious change both above and below the phase transition temperature. Qualitatively, the adhesion change can be understood from the structural changes from sc to fcc phases, in terms of the orientational-dependent van der Waals interaction and the short-range Coulomb interaction. Moreover, we have also studied the sliding velocity dependence of the friction and found a logarithmic velocity dependence in both phases below a critical scanning velocity. The scanning velocity-dependence measurement shows that the abrupt change in friction across the phase transition occurs at all velocities.

Acknowledgment. We wish to acknowledge the financial support of the Hong Kong University of Science and Technology through the William Mong Solid State Cluster Laboratory and the Postdoctoral Research Matching Fund as well as the support from the Research Grants Council of Hong Kong through Grant No. HKUST6164/01P. Y.X. and H.L. also acknowledge financial support from the NSFC (No. 10074053).

References and Notes

(1) Kroto, H. W.; Heath, J. R.; O'Brian, S. C.; Curl, R. F.; Smalley, R. E. *Nature* **1985**, *318*, 162.
(2) Curl, R. F.; Smalley, R. E. *Sci. Am.* **1991**, *256*, 54.
(3) David, W. I. F.; Ibberson, R. M.; Matthewman, J. C.; Prassides, K.; Dennis, T. J. S.; Hare, J. P.; Kroto, H. W.; Taylor, R.; Walton, D. R. W. *Nature* **1991**, *353*, 147.
(4) Johnson, R. D.; Yannoni, C. S.; Meijer, G.; Dorn, H. C.; Salem, J. R.; Bethune, D. S. *Science* **1992**, *255*, 1235.
(5) Heiney, P. A.; Fisher, J. E.; McGhie, A. R.; Romanow, W. J.; Denenstein, A. M.; McCauley, J. P., Jr.; Smith, A. B.; Cox, D. E. *Phys. Rev. Lett.* **1991**, *66*, 2911.
(6) Dresselhaus, M. S.; Dresselhaus, G.; Eklund, P. C. *Science of Fullerenes and Carbon Nanotubes*; Academic Press: San Diego, 1996.
(7) Harris, A. B.; Sachidanandam, R. *Phys. Rev. B* **1992**, *46*, 4944.
(8) David, W. I. F.; Ibberson, R. M.; Dennis, T. J. S.; Hare, J. P.; Prassides, K. *Europhys. Lett.* **1992**, *18*, 219.
(9) Carpick, R. W.; Salmeron, M. *Chem. Rev.* **1997**, *97*, 1163.
(10) Gao, J. P.; Luedtke, W. D.; Gourdon, D.; Ruths, M.; Israelachvili, J. N.; Landman, U. *J. Phys. Chem.* **2004**, *108*, 3410.
(11) Zhang, C.; Liang, Q.; Wang, B.; Xiao, X. D. *J. Appl. Phys.* **2004**, *95*, 3411.
(12) Bowden, F. B.; Tabor, D. *The friction and lubrication of solids, Part 2*; Clarendon: Oxford, 1964.
(13) Stolarski, T. A.; Tobe, S. *Rolling Contacts*; Professional Engineering Publishing Limited: London, 2000.
(14) Thundat, T.; Warmack, R. J.; Ding, D.; Compton, R. N. *Appl. Phys. Lett.* **1993**, *63*, 891.
(15) Schwarz, U. D.; Allers, W.; Gensterblum, G.; Wiesendanger, R. *Phys. Rev. B* **1995**, *52*, 14976.
(16) Bhushan, B.; Gupta, B. K.; Van Cleef, G. W.; Coe, J. V. *Appl. Phys. Lett.* **1993**, *62*, 3253.
(17) Okita, S.; Ishikawa, M.; Miura, K. *Surf. Sci.* **1999**, *442*, L959.
(18) Luengo, G.; Campbell, S. E.; Srdanov, V. I.; Wudl, F.; Israelachvili, J. N. *Chem. Mater.* **1997**, *9*, 1166.
(19) Mate, C. M. *Wear* **1993**, *168*, 17.
(20) Nakagawa, H.; Kibi, S.; Tagawa, M.; Umeno, M.; Ohmae, N. *Wear* **2000**, *238*, 45.
(21) Blau, P. J.; Haberlin, C. E. *Thin Solid Films* **1992**, *219*, 129.
(22) Mate, C. M.; McClelland, G. M.; Erlandsson, R.; Chiang, S. *Phys. Rev. Lett.* **1987**, *59*, 1942.
(23) Miura, K.; Kamiya, S. *Phys. Rev. Lett.* **2003**, *90*, 055509.
(24) Ren, S. L.; Yang, S. R.; Zhao, Y. *Langmuir* **2004**, *20*, 3601.
(25) Liang, Q.; Tsui, O. K. C.; Xu, Y. B.; Li, H. N.; Xiao, X. D. *Phys. Rev. Lett.* **2003**, *90*, 146102.
(26) Ogletree, D. F.; Carpick, R. W.; Salmeron, M. *Rev. Sci. Instrum.* **1996**, *67*, 3298.
(27) Hu, J.; Xiao, X. D.; Ogletree, D. F.; Salmeron, M. *Surf. Sci.* **1995**, *327*, 358.
(28) Tan, M. Q.; Xu, B.; Li, H. N.; Qi, Z. F.; Xu, Y. B. *J. Cryst. Growth* **1997**, *182*, 375.
(29) Yu, R. C.; Tea, N.; Salamon, M. B.; Lorents, D.; Malhotra, R. *Phys. Rev. Lett.* **1992**, *68*, 2050.
(30) Haluska, M.; Kuzmany, H.; Vybornov, M.; Rogl, P.; Fejdi, P. *Appl. Phys. A* **1993**, *56*, 161.
(31) Jiang, L.; Iyoda, T.; Li, J.; Kitazawa, K.; Fujishima, A.; Hashimoto, K. *J. Phys. Chem. B* **1998**, *102*, 6351.
(32) Schwarz, U. D.; Zworner, O.; Koster, P.; Wiesendanger, R. *Phys. Rev. B* **1997**, *56*, 6987.
(33) Qian, L. M.; Xiao, X. D. *Langmuir* **2000**, *16*, 662.
(34) Nioprobe Instruction Guide, Electron Microscopy Sciences, 2001.
(35) Williams, P. M.; Shakeshelf, K. M.; Davies, M. C.; Jackson, D. E.; Roberts, C. J.; Tendler, S. J. B. *J. Vac. Sci. Technol. B* **1996**, *14*, 1557.
(36) Howald, L.; Lüthi, R.; Meyer, E.; Güntherodt, H.-J. *Phys. Rev. B* **1995**, *51*, 5484.
(37) Park, J. Y.; Ogletree, D. F.; Salmeron, M.; Ribeiro, R. A.; Canfield, P. C.; Jenks, C. J.; Thiel, P. A. *Science* **2005**, *309*, 1354.
(38) Tsukruk, V. V.; Everson, M. P.; Lander, L. M.; Brittain, W. J. *Langmuir* **1996**, *12*, 3905.
(39) Johnson, K. L.; Kendall, K. K.; Roberts, A. D. *Proc. R. Soc., A* **1971**, *324*, 301.
(40) Meyer, E.; Overney, R. M.; Dransfeld, K.; Gyalog, T. *Nanoscience*, World Scientific: Singapore, 1998.
(41) Israelachvili, J. N. *Intermolecular and surface forces*; Academic Press: London, 1991.
(42) Dayo, A,; Alnasrallah, W.; Krim, J. *Phys. Rev. Lett.* **1998**, *80*, 1690.
(43) Renner, R. L.; Taborek, P.; Rutledge, J. E. *Phys. Rev. B* **2001**, *63*, 233405.
(44) Daly, C.; Krim, J. *Phys. Rev. Lett.* **1996**, *76*, 803.
(45) Tomassone, M. S.; Sokoloff, J. B.; Widom, A.; Krim, J. *Phys. Rev. Lett.* **1997**, *79*, 4798.
(46) Barrena, E.; Kopta, S.; Ogletree, D. F.; Charych, D. H.; Salmeron, M. *Phys. Rev. Lett.* **1999**, *82*, 2880.
(47) Lu, J. P.; Li, X.-P.; Martin, R. M. *Phys. Rev. Lett.* **1992**, *68*, 1551.
(48) Savin, S.; Harris, A. B.; Yildirim, T. *Phys. Rev. B* **1997**, 55, 14182.
(49) Gnecco, E.; Bennewitz, R.; Gyalog, T.; Loppacher, Ch.; Bammerlin, M.; Meyer, E.; Güntherodt, H.-J. *Phys. Rev. Lett.* **2000**, *84*, 1172.
(50) Fusco, C.; Fasolino, A. *Phys. Rev. B* **2005**, *71*, 45413.
(51) Riedo, E.; Levy, F.; Brune, H. *Phys. Rev. Lett.* **2002**, *88*, 185505.
(52) He, M. Y.; Blum, A. S.; Overney, G.; Overney, R. M. *Phys. Rev. Lett.* **2002**, *88*, 154302.
(53) Bouhacina, T.; Aime, J. P.; Gauthier, S.; Michel, D.; Heroguez, V. *Phys. Rev. B* **1997**, *56*, 7694.
(54) Zworner, O.; Holscher, H.; Schwarz, U. D.; Wiesendanger, R. *Appl. Phys. A* **1998**, *66*, 263.
(55) Gourdon, D.; Burnham, N. A.; Kulik, A.; Dupas, E.; Oulevey, F.; Gremaud, G.; Stamou, D.; Liley, M.; Dienes, Z.; Vogel, H.; Duschl, C. *Tribol. Lett.* **1997**, *3*, 317.